



Article

Fractional Order Fuzzy Dispersion Entropy and Its Application in Bearing Fault Diagnosis

Yuxing Li ^{1,2} , Bingzhao Tang ¹ , Bo Geng ¹ and Shangbin Jiao ^{1,2,*}¹ School of Automation and Information Engineering, Xi'an University of Technology, Xi'an 710048, China² Shaanxi Key Laboratory of Complex System Control and Intelligent Information Processing, Xi'an University of Technology, Xi'an 710048, China

* Correspondence: jiaoshangbin@xaut.edu.cn

Abstract: Fuzzy dispersion entropy (FuzzDE) is a very recently proposed non-linear dynamical indicator, which combines the advantages of both dispersion entropy (DE) and fuzzy entropy (FuzzEn) to detect dynamic changes in a time series. However, FuzzDE only reflects the information of the original signal and is not very sensitive to dynamic changes. To address these drawbacks, we introduce fractional order calculation on the basis of FuzzDE, propose FuzzDE_α , and use it as a feature for the signal analysis and fault diagnosis of bearings. In addition, we also introduce other fractional order entropies, including fractional order DE (DE_α), fractional order permutation entropy (PE_α) and fractional order fluctuation-based DE (FDE_α), and propose a mixed features extraction diagnosis method. Both simulated as well as real-world experimental results demonstrate that the FuzzDE_α at different fractional orders is more sensitive to changes in the dynamics of the time series, and the proposed mixed features bearing fault diagnosis method achieves 100% recognition rate at just triple features, among which, the mixed feature combinations with the highest recognition rates all have FuzzDE_α , and FuzzDE_α also appears most frequently.



Citation: Li, Y.; Tang, B.; Geng, B.; Jiao, S. Fractional Order Fuzzy Dispersion Entropy and Its Application in Bearing Fault Diagnosis. *Fractal Fract.* **2022**, *6*, 544. <https://doi.org/10.3390/fractalfract6100544>

Academic Editors: Viorel-Puiu Paun and António Lopes

Received: 9 August 2022

Accepted: 22 September 2022

Published: 26 September 2022

Publisher's Note: MDPI stays neutral with regard to jurisdictional claims in published maps and institutional affiliations.



Copyright: © 2022 by the authors. Licensee MDPI, Basel, Switzerland. This article is an open access article distributed under the terms and conditions of the Creative Commons Attribution (CC BY) license (<https://creativecommons.org/licenses/by/4.0/>).

Keywords: fuzzy dispersion entropy; fractional order; feature extraction; bearing fault diagnosis

1. Introduction

Entropy, as a measure of time series disorder and predictability, can evaluate the complexity of the signal [1,2]. The greater the entropy value, the higher the complexity of signal [3,4]. In recently years, entropy has been widely applied in mechanical fault diagnosis and has shown excellent performance [5–7].

Dispersion entropy (DE) divides time series into integer series by introducing different mapping criteria for the first time [8], which enables it to capture more amplitude information than permutation entropy (PE) and sample entropy (SE) [9,10]. Some scholars have made every attempt to study the improved version of DE to further enhance its performance as a complexity index. Fluctuation-based DE (FDE) and reverse DE (RDE) have also been proposed by introducing fluctuation information and distance information between time series and white noise [11–13]. In 2021, by combining the fluctuation information of FDE and the distance information of RDE [14], the reverse DE (FRDE) based on fluctuation is proposed, which has better stability and discrimination ability for different types of time series.

Fuzzy dispersion entropy (FuzzDE) is a new method proposed in 2021 [15], which combines the advantages of fuzzy entropy (FuzzEn) as well as DE by replacing the round mapping function of DE with fuzzy membership function in FuzzEn, by which the dynamic changes of time series can be retained to a greater extent and the problem of missing useful information brought about by round mapping function can be alleviated. Nevertheless, the FuzzDE still suffers from the same problem of single feature as common entropies, which cannot characterize the time series from multiple fractional orders.

To address the problem of single fractional order, in recent years, many scholars have conducted research on the application of fractional order calculation to entropy [16–18]. In

2019, the fractional fuzzy entropy algorithm was proposed and used for physiological and biomedical analysis of EEG signals [19]. In 2020, generalized refined composite multiscale fluctuation-based fractional dispersion entropy (GRCMFDE_α) combined refined composite multiscale dispersion entropy (RCMDE) as well as fractional order calculation and was applied for bearing signal fault diagnosis with good results [20]. In 2022, fractional order calculation was introduced to slope entropy to effectively diagnose the location and severity of faults in rolling bearings [21].

Inspired by these works, we introduce fractional order calculation into FuzzDE in this paper, and fractional order FuzzDE (FuzzDE_α) is proposed. Compared with FuzzDE, FuzzDE_α further considers fractional order information and measures the dynamic changes of time series from multiple fractional orders. In addition, we combine FuzzDE_α with other fractional order entropies and propose a mixed feature bearing fault diagnosis method. Simulated as well as real-world experiments demonstrate the sensitivity of FuzzDE_α to the dynamic changes of time series and the excellent performance on bearing fault diagnosis.

The rest of this paper is organized as follows: Section 2 presents the theoretical steps of FuzzDE_α and discusses the parameter settings; Section 3 experiments on the effectiveness of fractional order on FuzzDE through simulated signals; Section 4 validates the bearing fault diagnosis capability of FuzzDE_α through real-world bearing signals; Section 5 concludes the whole paper.

2. Fractional Order Fuzzy Dispersion Entropy

2.1. FuzzDE_α

FuzzDE_α is the introduction of the concept of fractional order calculation on the basis of FuzzDE, for a given time series $X = \{x_1, x_2, \dots, x_N\}$ of length N , the specific steps for FuzzDE_α can be expressed as follows:

Step 1: By applying the normal cumulative distribution function (NCDF) to the original time series X , $Y = \{y_1, y_2, \dots, y_N\}$ can be derived with the interval $[-1, 1]$, where the NCDF can be expressed as follows:

$$y_i = \frac{1}{\sigma\sqrt{2\pi}} \int_{-\infty}^{x_i} e^{-\frac{(t-\gamma)^2}{2\sigma^2}} dt \quad (i = 1, 2, \dots, N)$$

where σ and γ represent the standard deviation and mean of X , respectively.

Step 2: Normalize the sequence Y by converting each element in Y to the interval $[0, 1]$:

$$s_i = \frac{y_i}{Max - Min} \quad (i = 1, 2, \dots, N)$$

in which $S = \{s_1, s_2, \dots, s_N\}$ is the normalized sequence, Max and Min are the maximum and minimum values of the sequence Y , respectively.

Step 3: Introduce the class number c to convert the sequence S into a new sequence Z^c [15]:

$$z_i^c = cy_i + 0.5 \quad (i = 1, 2, \dots, N)$$

where each element z_i^c ($i = 1, 2, \dots, N$) in Z^c is in the interval $[0.5, c + 0.5]$.

Step 4: Introduce the embedding dimension m and time delay τ , reconstruct the sequence Z^c of Step 3 into $N - (m + 1)\tau$ subsequences $Z_j^{m,c}$:

$$Z_j^{m,c} = \{z_j^c, z_{j+(1)\tau}^c, \dots, z_{j+(m-1)\tau}^c\} \quad (j = 1, 2, \dots, N - (m + 1)\tau) \quad (1)$$

where m determines the number of elements contained in each subsequence $Z_j^{m,c}$, and τ determines the interval between two adjacent elements in the sequence Z^c .

Step 5: Introduce the fuzzy membership function on the sequence Z^c as follows:

$$\mu_{M_1}(z_i^c) = \begin{cases} 0 & z_i^c > 2 \\ 2 - z_i^c & 1 \leq z_i^c \leq 2 \\ 1 & z_i^c < 1 \end{cases}$$

$$\mu_{M_k}(z_i^c) = \begin{cases} 0 & z_i^c > k + 1 \\ k + 1 - z_i^c & k \leq z_i^c \leq k + 1 \\ z_i^c - k + 1 & k - 1 \leq z_i^c \leq k \\ 0 & z_i^c < k - 1 \end{cases} \quad (k = 2, 3, \dots, c - 1)$$

$$\mu_{M_c}(z_i^c) = \begin{cases} 1 & z_i^c > c \\ z_i^c - c + 1 & c - 1 \leq z_i^c \leq c \\ 0 & z_i^c < c - 1 \end{cases}$$

where k stands for the k th class, and M_k is the fuzzy membership function, $\mu_{M_k}(z_i^c)$ represents the degree of membership of z_i^c for the k th class. By the fuzzy membership function, each z_i^c will have 1 or 2 different degrees, and the value range is an integer between $[1, c]$, which is the same as the rounding function in the DE [8], but reduces the information loss in the rounding function. Figure 1 shows the fuzzy membership function.

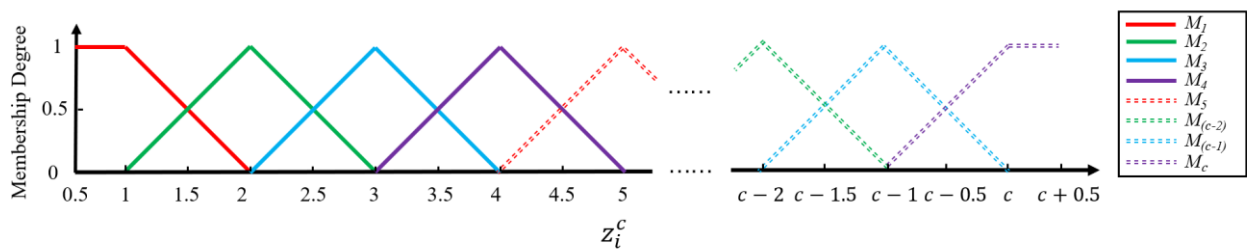


Figure 1. Fuzzy membership function.

Step 6: After the processing of the sequence Z^c in Step 5, each subsequence $Z_j^{m,c}$ can be mapped into a number of new sequences consisting of integers, and these sequences can be represented by the dispersion patterns $\pi_{v_0 v_1 \dots v_{m-1}}$, where v_0, v_1, v_{m-1} correspond to the integer values of $z_j^c, z_{j+(1)\tau}^c$, and $z_{j+(m-1)\tau}^c$ in Equation (1) after fuzzy processing, respectively.

Step 7: Calculate the degree of membership of each $Z_j^{m,c}$ with respect to the dispersion patterns $\pi_{v_0 v_1 \dots v_{m-1}}$ and denote as $\mu_{\pi_{v_0 v_1 \dots v_{m-1}}}$:

$$\mu_{\pi_{v_0 v_1 \dots v_{m-1}}}(z_j^{m,c}) = \prod_{i=0}^{m-1} \mu_{M_{v_i}}(z_{j+(i)\tau}^c)$$

in this manner, each subsequence $Z_j^{m,c}$ will correspond to multiple dispersion patterns accompanied by different membership degrees. For an example, given a subsequence $Z_1^{2,3} = [1.149, 2.306]$, all the membership degrees can be organized as follows:

$$\begin{cases} \mu_{M_1}(z_1^3) = 0.851 \\ \mu_{M_2}(z_1^3) = 0.149 \\ \mu_{M_2}(z_2^3) = 0.694 \\ \mu_{M_3}(z_2^3) = 0.306 \end{cases} \rightarrow \begin{cases} \mu_{\pi_{12}}(Z_1^{2,3}) = \mu_{M_1}(z_1^3) \times \mu_{M_2}(z_2^3) = 0.5906 \\ \mu_{\pi_{13}}(Z_1^{2,3}) = \mu_{M_1}(z_1^3) \times \mu_{M_3}(z_2^3) = 0.2604 \\ \mu_{\pi_{22}}(Z_1^{2,3}) = \mu_{M_2}(z_1^3) \times \mu_{M_2}(z_2^3) = 0.1034 \\ \mu_{\pi_{23}}(Z_1^{2,3}) = \mu_{M_2}(z_1^3) \times \mu_{M_3}(z_2^3) = 0.0456 \end{cases}$$

Step 8: The frequency of each dispersion pattern $p(\pi_{v_0, v_1, \dots, v_{m-1}})$ can be calculated:

$$p(\pi_{v_0, v_1, \dots, v_{m-1}}) = \frac{\sum_{j=1}^{N-(m-1)d} \mu_{\pi_{v_0, v_1, \dots, v_{m-1}}}(\mathbf{z}_j^{m,c})}{N - (m-1)\tau}$$

Step 9: For writing convenience, we define $p(\pi_{v_0, v_1, \dots, v_{m-1}})$ as P_j . Then the fractional order calculation is applied, and the FuzzDE $_{\alpha}$ can be expressed as [20]:

$$\text{FuzzDE}_{\alpha}(X, m, c, \tau) = \sum_j P_j \left\{ -\frac{P_j^{-\alpha}}{\Gamma(\alpha+1)} [\ln P_j + \psi(1) - \psi(1-\alpha)] \right\}$$

where α is the order of fractional derivative. $\Gamma(\cdot)$ and $\psi(\cdot)$ denote the gamma function and digamma function respectively.

Step 10: The normalized form NFuzzDE $_{\alpha}$ of FuzzDE $_{\alpha}$ can be computed as:

$$\text{NFuzzDE}_{\alpha}(X, m, c, \tau) = \frac{\text{FuzzDE}_{\alpha}(X, m, c, \tau)}{\ln(c^m)}$$

2.2. Parameter Selection

In this subsection, we mainly focus on the discussion of the parameter selection for FuzzDE $_{\alpha}$. For the parameter comparison experiments, 50 separate groups of pink noises, white noises and blue noises are selected [20], each with 2048 sample points. Where white noise consists of a homogeneous mixture of signals of different frequencies, with a variety of frequencies in a haphazard manner. Pink noise enhances the sound intensity of low frequency signals and weakens the intensity of high frequency signals compared to white noise, while blue noise, in contrast, enhances the sound intensity of the high frequency signal on top of the white noise. Using the control variables method, the effects of three FuzzDE $_{\alpha}$ parameters, namely the number of classes c , the embedding dimension m and the mapping method, on the mean as well as the standard deviation of the selected noise signals are explored as shown in Figures 2–4, respectively.

To begin with, we conduct comparative experiments on the effects of c , and the interval is set to an integer between 2 and 5 ($m = 3$, mapping as NCDF), Figure 2 shows the means and standard deviations of different class number c at different fractional orders.

Comparing the four images, it can be seen that for the average of the entropy values of the three noises, the trend when m equals 3 and c equals 2 is different from the other three in that it has a slope from large to small, while the others are from small to large. However, the general trend is that it increases with the increase of α . For the standard deviation of the entropy values of the three noise entropy values, the standard deviation of the pink noise is larger, and the others are smaller, and as α increases, the value of the standard deviation also increases, which is especially evident in the pink noise. In summary, changes in c have an impact on the magnitude of entropy value, but the overall trend in entropy value and the ability to discriminate between different noises does not change as the fractional order changes.

We next discuss the effect of m , with the interval set to an integer between 3 and 6 ($c = 3$, mapping as NCDF), Figure 3 is means and standard deviations of different embedding dimensions m at different fractional orders.

Observing the four subplots, for the average of the FuzzDE $_{\alpha}$ values of the three noises, all four cases of taking values show a similar upward trend. For the standard deviation of the entropy values of the three noises, there is only a difference between the exact values and the overall trend is almost the same. Thus, it is clear that the effect of m has a greater impact on the magnitude of the entropy value compared to c , but the overall trend and the ability to distinguish between different noises does not change.

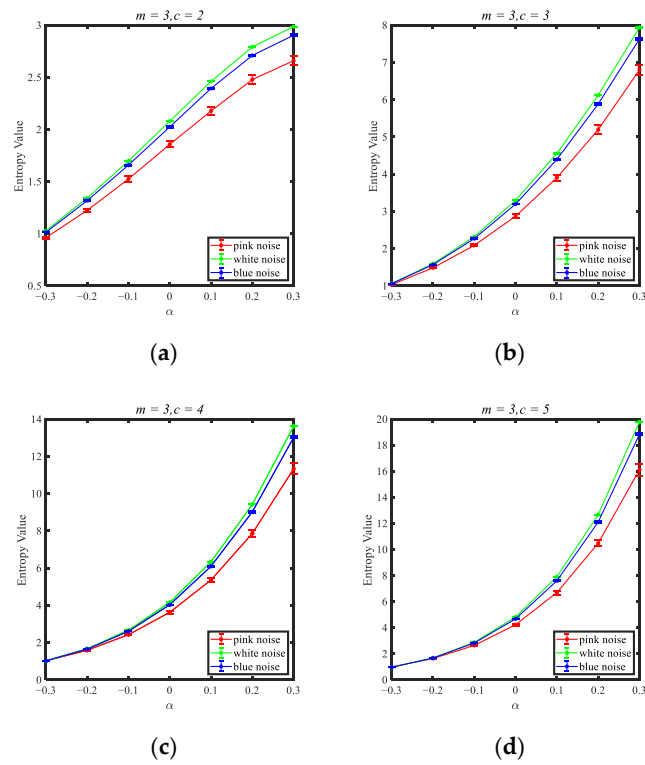


Figure 2. Means and standard deviations of different class number c at different fractional orders. (a) $c = 2$; (b) $c = 3$; (c) $c = 4$; (d) $c = 5$.

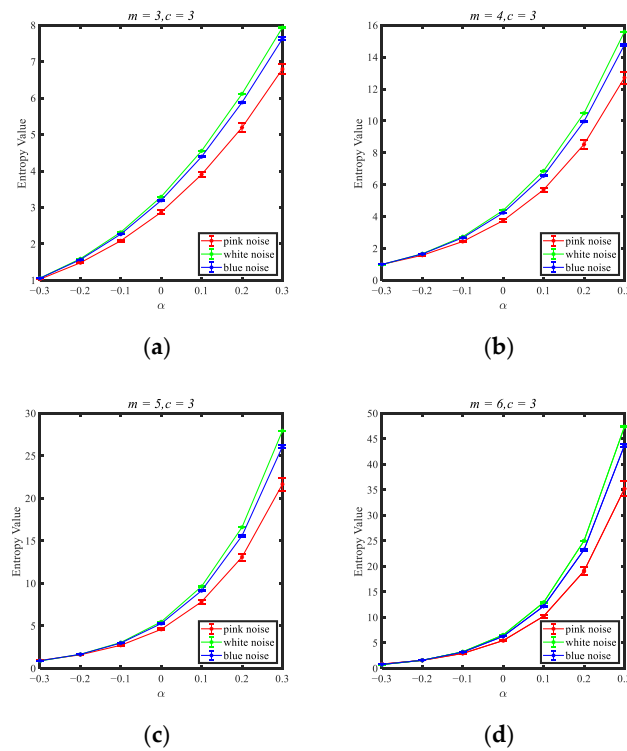


Figure 3. Means and standard deviations of different embedding dimensions m at different fractional orders. (a) $m = 3$; (b) $m = 4$; (c) $m = 5$; (d) $m = 6$.

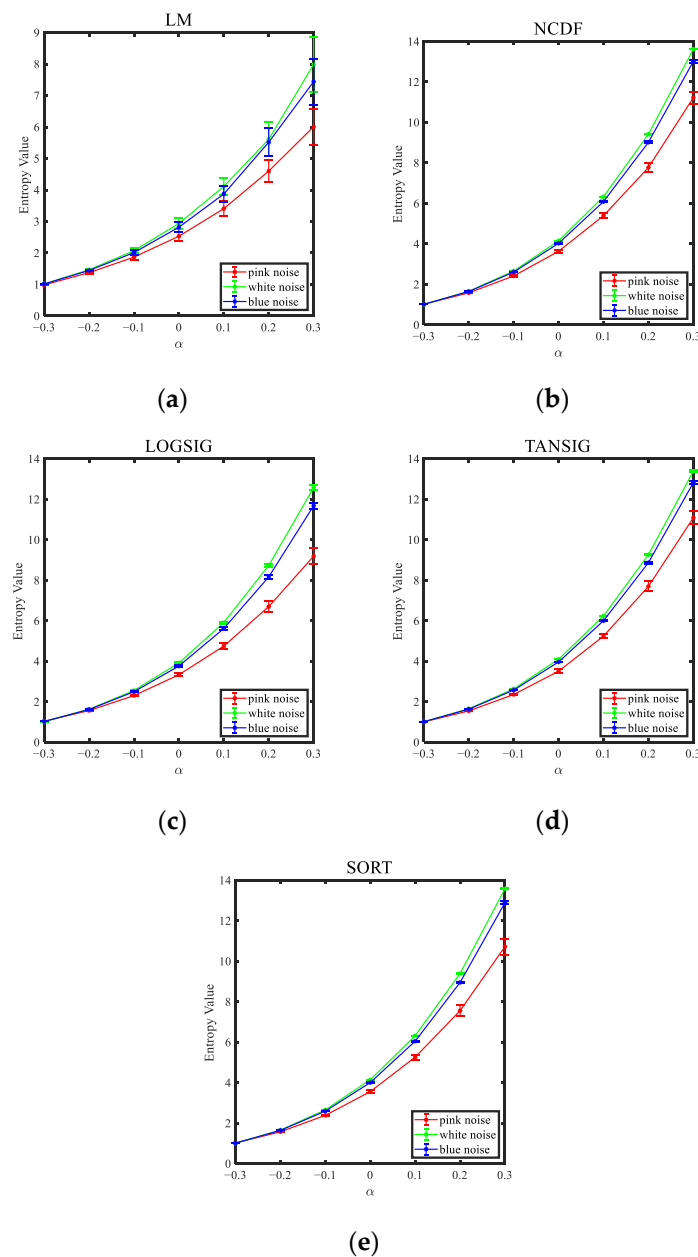


Figure 4. Means and standard deviations of different mapping approaches at different fractional orders. (a) LM; (b) NCDF; (c) LOGSIG; (d) TANSIG; (e) SORT.

Finally, we discuss the effect of the mapping method, which is also an important influencing factor, so we choose different mapping methods for comparison. Figure 4 shows the means and standard deviations of different mapping approaches at different fractional orders, among which the mapping methods include linear mapping (LM), normal cumulative distribution function (NCDF), tangent sigmoid (TANSIG), logarithm sigmoid (LOGSIG), and sorting method (SORT) respectively ($c = 3, m = 3$) [8–11].

According to Figure 4, the overall trends of the five mapping methods are very similar, but when using the LM mapping method, the standard deviation of the various noise entropy values is significantly larger, accompanied by the condition that the various noise entropy values overlap each other, which indicates that when the selected mapping method is LM, the stability of $FuzzDE_\alpha$ after mapping is relatively weak, and it is difficult to distinguish the three types of noise. While the standard deviation of other mapping methods is relatively small. Therefore, it is concluded that NCDF, LOGSIG, TANSIG or SORT are the recommended mapping approaches.

In conclusion, m and c have little effect on the experiment, but a large m is more likely to lead to an increase in FuzzDE_α values compared to c . Among all mapping methods, only LM is not stable. Therefore, we recommend that m be set to 3–6, c to 2–5 and the mapping method be NCDF, LOGISG, TANSIG or SORT. In the later simulations and the real-world signal experiments, we choose $m = 3$, $c = 4$ and the mapping method to be NCDF.

3. Experiments on Simulated Signals

In this section, we focus on demonstrating the usefulness of fractional order calculations on FuzzDE by simulated signals, mainly including noise signals, chirp signal and MIX signal.

3.1. Noise Signals Experiment

In order to verify the effectiveness of fractional order calculation on FuzzDE, pink noise, white noise and blue noise are selected for comparative experiments, and the fractional orders change from -0.5 to 0.5 with interval 0.1 . 100 independent pink noises, white noises and blue noises are created to prove the discrimination ability of fractional order. The means and standard deviations of these 100 FuzzDE_α values are calculated respectively as displayed in Figure 5.

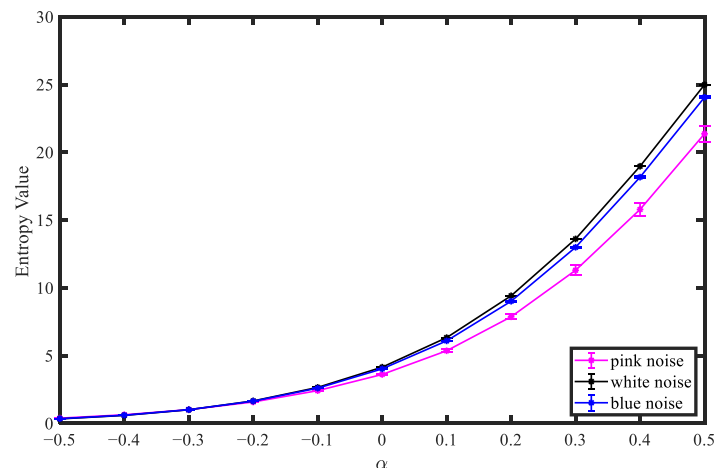


Figure 5. Means and standard deviations of different fractional order entropies under noise signals.

As shown in Figure 5, the FuzzDE_α value of the three kinds of noise signals has a similar upward trend with the increase of fractional order; when the fractional order is less than -0.1 , the mean characteristics of the three noise signals are mixed together; when the fractional order is greater than -0.1 , the difference of mean characteristics of the three noise signals gradually increases, and the FuzzDE_α value of white noise is the largest, with the smallest standard deviation and the most stable FuzzDE_α value. Experiments show that as the fractional order increases (when the fractional order is greater than -0.1), FuzzDE_α has a better distinguishing effect on pink noise, white noise and blue noise.

3.2. Chirp Signal Experiment

Chirp signal is a typical unstable signal, and frequency of chirp signal will change over time [22,23]. In order to better show the feature extraction effect of FuzzDE_α at different fractional orders, chirp signal is used for simulated experiments. Chirp signal can be expressed as:

$$x(t) = e^{(j2\pi(f_0t + \frac{1}{2}kt^2))}$$

where f_0 is the initiation frequency and is taken as 20 Hz, k is the modulation frequency and is taken as 3, we can understand that the frequency increases from 20 Hz to 80 Hz. The chirp signal lasts 20 s with a sampling frequency of 1000 Hz (20,000 sampling points).

We take the length of the sliding window as 1000 sampling points, and slide backward from the first sampling point with 90% overlap to obtain 190 samples. FuzzDE $_{\alpha}$ for chirp signal of each sample are calculated. Chirp signal (top) and the corresponding different entropy curves (bottom) are shown in Figure 6.

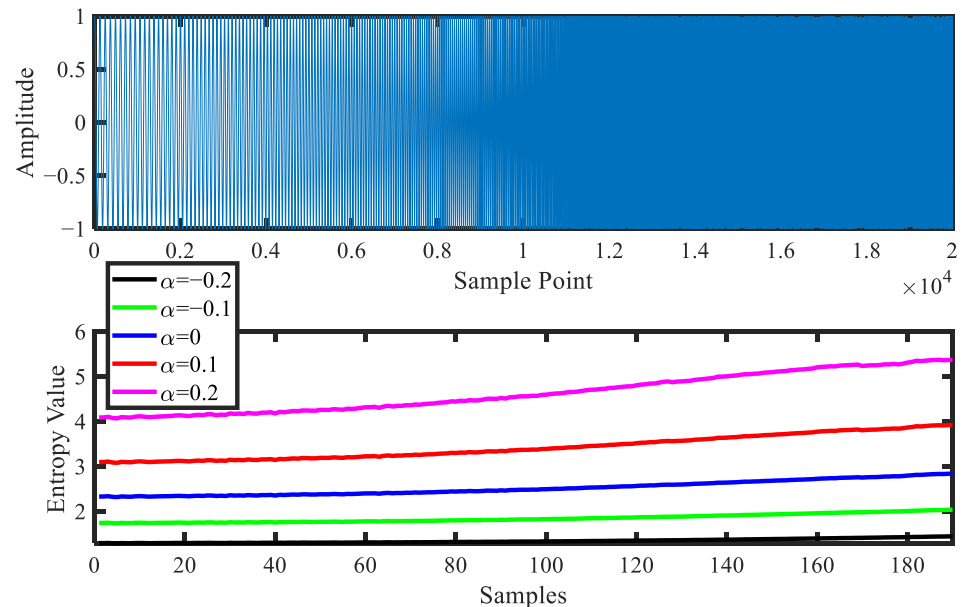


Figure 6. Chirp signal (top) and the corresponding different entropy curves (bottom).

It can be observed from Figure 6 that the waveform of the chirp signal gradually becomes denser as the number of sampling points increases, and the higher the fractional order, the larger the FuzzDE $_{\alpha}$ value as well as the rate of increase of the curve. In a word, the experimental results show that the higher the fractional order of FuzzDE $_{\alpha}$, the better performance of FuzzDE $_{\alpha}$ in chirp signal feature extraction.

3.3. MIX Signal Experiment

In order to study the influence for fractional order of FuzzDE $_{\alpha}$ on the effect of feature extraction, we select MIX signal for simulated experiments. MIX signal describes a stochastic sequence that progressively turns into a periodic time series [24,25], which can be expressed as:

$$\begin{cases} MIX(t) = (1 - Z) \times X(t) + Z \times Y(t) \\ X(t) = \sqrt{2} \sin \frac{2\pi t}{12} \end{cases}$$

where $X(t)$ is a periodic signal, the value of $Y(t)$ is uniformly distributed from $-\sqrt{3}$ to $\sqrt{3}$, and Z is a random number taking 1 or 0 with probabilities P and $1 - P$, respectively, and decreasing linearly from 0.99 at the beginning to 0.01 at the end. The sampling frequency of mix signal is 1000 Hz, with a total of 20 s. We take the length of sliding window as 1000 sampling points, and slide backward from the first sampling point with 90% overlap to obtain 190 samples. MIX signal (top) and the corresponding different entropy curves (bottom) are shown in Figure 7.

As can be seen from Figure 7, the MIX signal changes from dense to sparse as the number of sampling points increases; the value of FuzzDE $_{\alpha}$ decreases as the number of sampling points increases; the higher the fractional order, the larger the FuzzDE $_{\alpha}$ value and the rate of decline of the curve also increases. Therefore, we can conclude that an increase in fractional order can better reflect the complexity of the MIX signal.

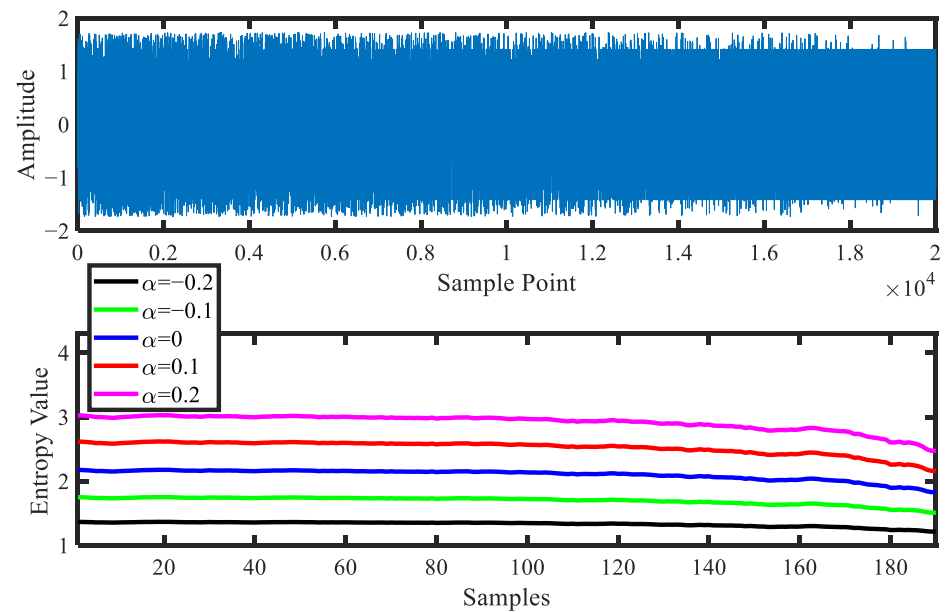


Figure 7. MIX signal (top) and the corresponding different entropy curves (bottom).

4. Experiments on Bearing Fault Diagnosis

In this section, we focus on the bearing fault diagnosis, and achieve early prevention in order to avoid economic losses and even personal safety due to different bearing faults. Since entropy can be used to detect changes in the dynamics of weak time series, the higher the entropy value, the more unstable the time series and vice versa. At the same fault size, different faults have similar amplitude-frequency features, but their bearing fault complexity and dynamics changes are different, and these changes can be reflected in successive subsequences, for which entropy features can be extracted for fault diagnosis of the bearing signals. The experiments in this section are mainly to verify the effectiveness of FuzzDE $_{\alpha}$ for bearing fault diagnosis, and the proposed mixed features bearing fault diagnosis method experimental flow chart is shown in Figure 8, with the following steps:

Step 1: Input the real-world bearing signals of ten different classes.

Step 2: Segment the input signals into M samples, each with N sample points, by which way, we receive a total of M samples for each class of signal.

Step 3: For each sample, calculate their FuzzDE $_{\alpha}$ values at different fractional orders. For the purpose of contrast, we also introduce fractional order DE (DE $_{\alpha}$), fractional order PE (PE $_{\alpha}$) and fractional order FDE (FDE $_{\alpha}$) for comparison, with fractional orders of -0.2 , -0.1 , 0 , 0.1 , and 0.2 respectively.

Step 4: Mix the 20 features obtained in Step 3 and set the number of selected features to K (initialized to 2), by which way we can acquire a total of C_{20}^K combinations.

Step 5: Calculate the recognition rate of all C_{20}^K combinations and select the combination with the highest recognition rate.

Step 6: Determine the direction of the process by the number of features selected, and if $K < 5$, skip to Step 7; otherwise, output the combination of 5 features with the highest recognition rate and the corresponding recognition rate, as a way to avoid the increased computational consumption when the recognition rate has reached the threshold.

Step 7: Determine the direction of the process by the highest recognition rate among K feature combinations. If the recognition rate reaches 100%, then output these feature combinations; otherwise, let $K = K + 1$ and back to Step 5.

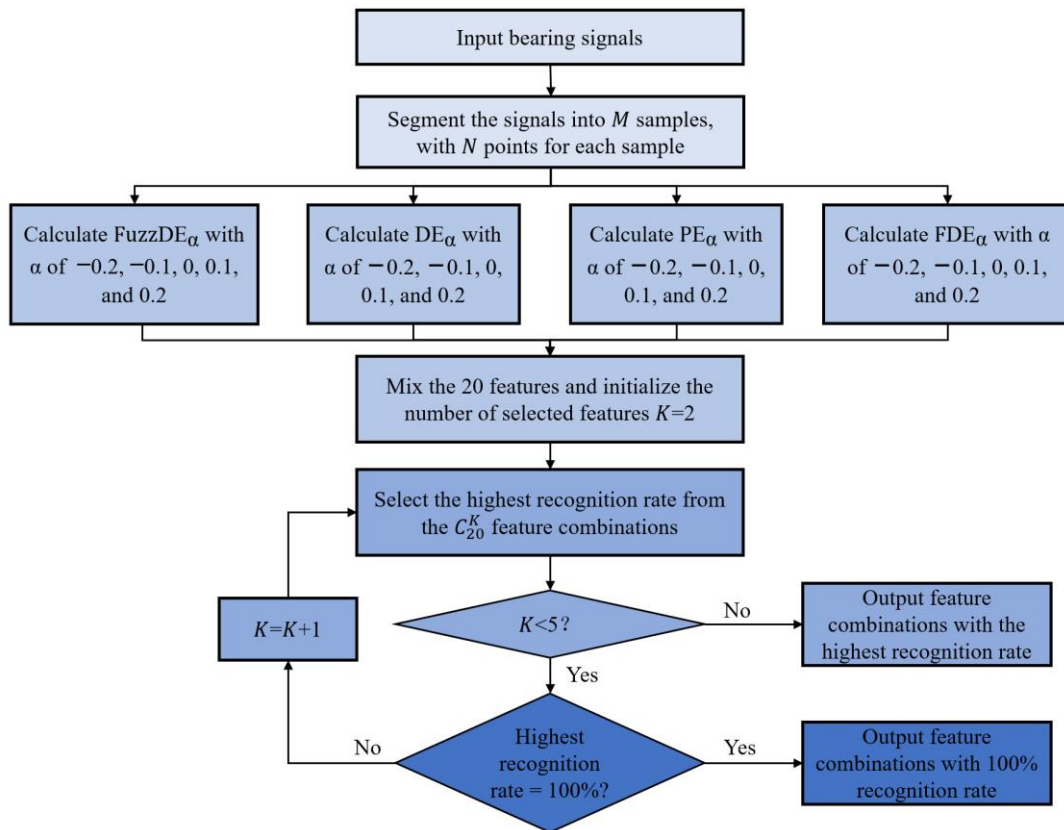


Figure 8. Flow chart of the proposed mixed features bearing fault diagnosis method.

4.1. Analysis of Experiment Data

This section employs the bearing signal obtained from Case Western Reserve University (CWRU) [26] to verify the effectiveness of the proposed FuzzDE α . The bearing under test is a deep groove ball bearing type SKF6205 (CWRU, Cleveland, America) with a motor speed set to 1730 r/min and a load of 3 hp. The original bearing signal is acquired by collecting the acceleration sensor installed at the driving end, and the sampling frequency is 12 kHz. Depending on the states of the bearing and the diameters of the failure, there are 10 different types of bearing signals marked NORM, IR1, BE1, OR1, IR2, BE2, OR2, IR3, BE3 and OR3, all damage is caused by electro discharge machining as a single point of damage. The details of the selected bearing signals are shown in Table 1. For each class of bearing signal, the length of sample points is 120,000, and Figure 9 shows the time domain distribution of ten classes of bearing signals.

Table 1. Details of the selected bearing signals.

Class	Label	Fault Size (mm)	Selected Data
Normal	NORM	0	100_normal_3
Inner race fault	IR1	0.1778	108_IR007_3
Balling element fault	BE1	0.1778	121_B007_3
Outer race fault	OR1	0.1778	133_OR007@6_3
Inner race fault	IR2	0.3556	172_IR014_3
Balling element fault	BE2	0.3556	188_B014_3
Outer race fault	OR2	0.3556	200_OR014@6_3
Inner race fault	IR3	0.5334	212_IR021_3
Balling element fault	BE3	0.5334	225_B021_3
Outer race fault	OR3	0.5334	237_OR021@6_3

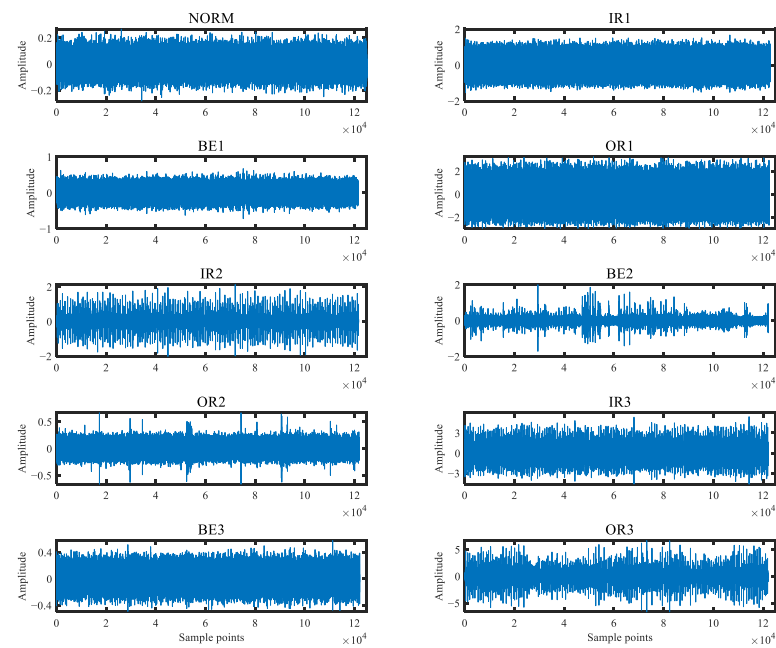


Figure 9. Time domain distribution of ten classes of bearing signals.

4.2. Single Feature Extraction and Classification

The ten classes of bearing signals are used as the object of the experiment for single feature extraction. There are 50 samples for each type of bearing signal, and each sample contains 2048 sample points. While calculating the $FuzzDE_{\alpha}$ of the bearing signal, the DE_{α} , PE_{α} , and FDE_{α} are calculated respectively as comparative analysis. The parameter settings are as follows: embedding dimension m is 3, class number c is 4, and the range of fractal order α is from -0.2 to 0.2 with interval 0.1 . For other fractional entropies, the parameter settings are the same as $FuzzDE_{\alpha}$. The Distribution of fractional entropy features of different classes of bearing signals are exhibited in Figure 10.

From Figure 10, for the four types of fractional entropies, it is difficult to completely distinguish all ten types of bearing signals under different fractional order; for $FuzzDE_{\alpha}$, DE_{α} , and FDE_{α} , there is always some standard deviation of fractional entropy values close to each other for bearing signals; in addition, the standard deviation of fractional entropy values are significantly higher than that of PE_{α} under different fractional order, for PE_{α} , the standard deviations of fractional entropy values for ten classes of bearing signals are all very close, which is difficult to distinguish. Furthermore, we employ KNN to classify the ten classes of bearing signals, in which there are 50 samples for each type of bearing signal, the first 25 samples are training samples, and the rest samples are test samples. Table 2 illustrates the classification recognition rate of different entropies at various fractional orders.

Table 2. Classification recognition rate of different entropies at various fractional orders.

Entropy	Recognition Rates (%)				
	$\alpha=-0.2$	$\alpha=-0.1$	$\alpha=0$	$\alpha=0.1$	$\alpha=0.2$
$FuzzDE_{\alpha}$	82.8	81.6	74	68.4	67.6
DE_{α}	76.4	79.6	76.4	71.2	66.0
PE_{α}	59.6	56.8	58.4	56.8	54.0
FDE_{α}	79.2	82.8	78.4	77.6	80.4

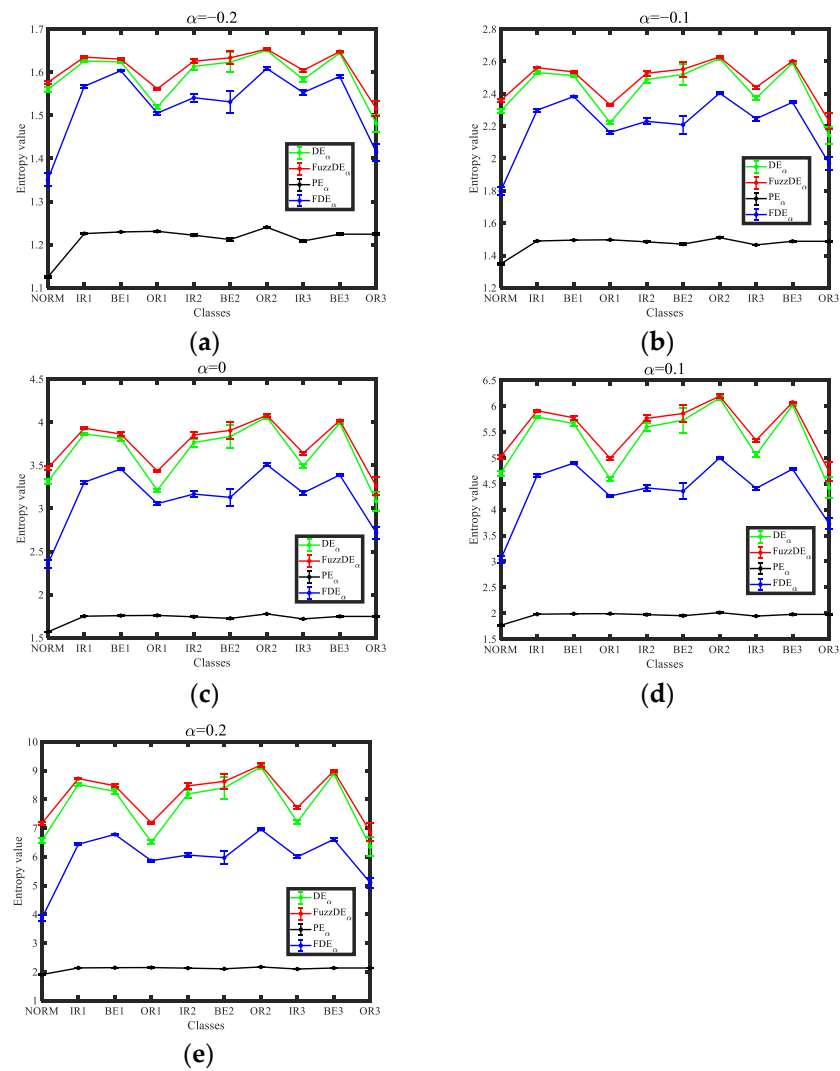


Figure 10. Distribution of fractional entropy features of different classes of bearing signals. (a) $\alpha = -0.2$; (b) $\alpha = -0.1$; (c) $\alpha = 0$; (d) $\alpha = 0.1$; (e) $\alpha = 0.2$.

It can be seen from Table 2, for four classes of fractional entropies, the recognition rates of bearing signals are all lower than 85% under different fractional orders, and the recognition effect is poor. Therefore, it is difficult to distinguish ten classes of signals with one feature.

4.3. Double Features Extraction and Classification

In order to improve recognition performance and demonstrate the effectiveness of the mixed feature extraction method proposed in this paper, we choose different entropy-based feature extraction methods, extract any two fractional orders with the same entropy and choose the best combinations of fractional orders. Since fractional order α has 5 values, a total of C_5^2 combinations can be obtained by each entropy-based feature extraction method. In addition, we use the mixed feature extraction method proposed in this paper to calculate the highest recognition rate, with a total of C_{20}^2 combinations. Table 3 demonstrate the highest classification recognition rates for each feature extraction method when double features are selected.

Table 3. Highest classification recognition rates for each feature extraction method (double features).

Feature Extraction Methods	Combinations	Recognition Rate (%)
FuzzDE $_{\alpha}$ -based	FuzzDE $_{\alpha=0}$ & FuzzDE $_{\alpha=0.2}$	91.6
DE $_{\alpha}$ -based	DE $_{\alpha=0}$ & DE $_{\alpha=0.2}$	88.4
PE $_{\alpha}$ -based	PE $_{\alpha=-0.2}$ & PE $_{\alpha=0.1}$	58.4
FDE $_{\alpha}$ -based	FDE $_{\alpha=-0.1}$ & FDE $_{\alpha=0}$	90.0
Proposed method	FuzzDE $_{\alpha=0.1}$ & FDE $_{\alpha=0.1}$ (1 of 3)	99.6

In Table 3, FuzzDE $_{\alpha=0}$ & FuzzDE $_{\alpha=0.2}$ represents FuzzDE $_{\alpha}$ when fractional order α is 0 and 0.2 respectively, other combinations of entropy are the same for FuzzDE $_{\alpha=0}$ & FuzzDE $_{\alpha=0.2}$. As can be observed in Table 3, FuzzDE $_{\alpha}$ -based feature extraction method has the best classification effect among the four entropy-based feature extraction methods, but the highest recognition rate is only 91.6%, which cannot fully recognize the bearing signals. Nevertheless, the mixed feature extraction method proposed in this paper can reach a maximum classification rate of 99.6%, significantly higher than the 91.6% of FuzzDE $_{\alpha}$ -based feature extraction method, and there are three combinations in total, namely FuzzDE $_{\alpha=0.1}$ & FDE $_{\alpha=0.1}$, FuzzDE $_{\alpha=-0.1}$ & FDE $_{\alpha=0.1}$ and FuzzDE $_{\alpha=0.1}$ & FDE $_{\alpha=-0.1}$. It is noteworthy that when reaching the highest recognition rate, the three combinations all contain FuzzDE $_{\alpha}$, which further proves the importance of FuzzDE $_{\alpha}$ in bearing fault diagnosis recognition. Figure 11 shows the distribution of the highest classification recognition rate of mixed double features.

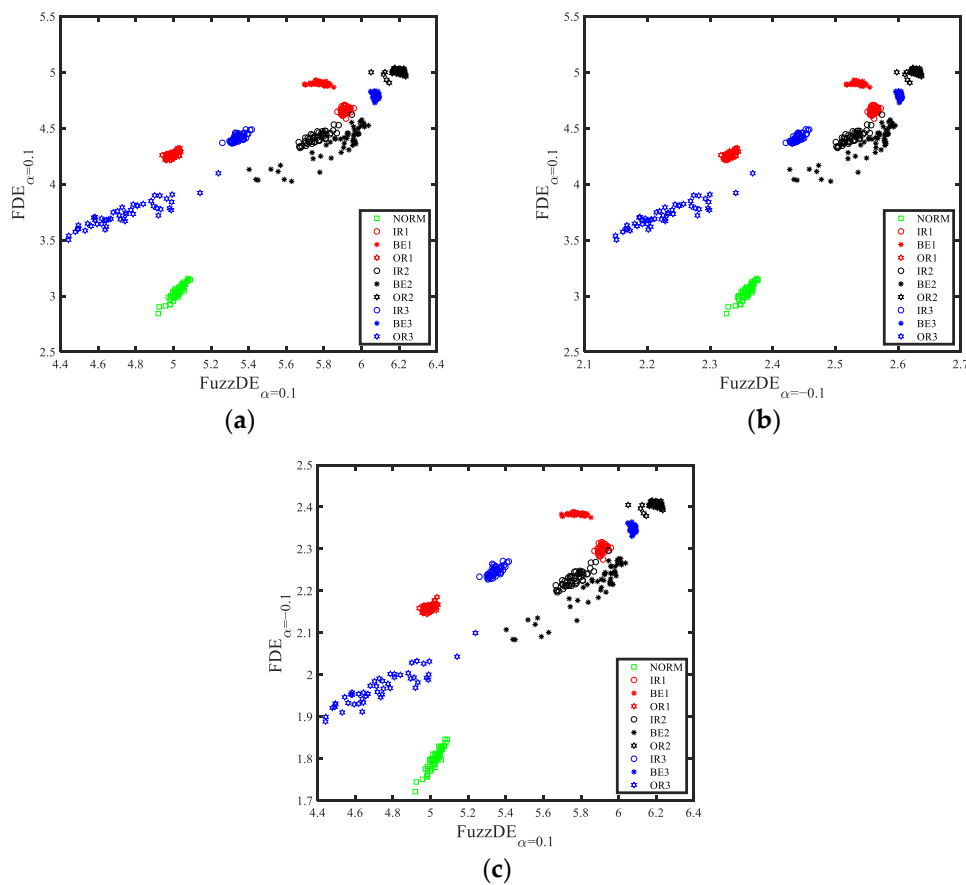


Figure 11. Distribution of the highest classification recognition rate of mixed double features. (a) FuzzDE $_{\alpha=0.1}$ & FDE $_{\alpha=0.1}$; (b) FuzzDE $_{\alpha=-0.1}$ & FDE $_{\alpha=0.1}$; (c) FuzzDE $_{\alpha=0.1}$ & FDE $_{\alpha=-0.1}$.

As can be seen from Figure 11, under the mixed double features, the distribution of each type of bearing signal is relatively concentrated, and the overlapping part is very

small. However, there are few samples that are not completely distinguishable, for example, a small percentage of IR1 and IR2 samples are mixed. In summary, compared with the entropy-based feature extraction methods, the mixed feature extraction method proposed in this paper further improves the recognition rate and can better distinguish the ten classes of bearing signals. To sum up, mixed double features extraction method can well distinguish the ten classes of bearing signals.

4.4. Triple Features Extraction and Classification

In order to further improve the recognition rate of bearing fault diagnosis, we set the number of selected features H to 3. The rest of the steps are the same as Section 4.3, and Table 4 shows the highest classification recognition rates for each feature extraction method when triple features are selected.

Table 4. Highest classification recognition rates for each feature extraction method (triple features).

Feature Extraction Methods	Combinations	Recognition Rate (%)
FuzzDE $_{\alpha}$ -based	FuzzDE $_{\alpha=-0.1}$ & FuzzDE $_{\alpha=0}$ & FuzzDE $_{\alpha=0.2}$	92
DE $_{\alpha}$ -based	DE $_{\alpha=-0.1}$ & DE $_{\alpha=0}$ & DE $_{\alpha=0.2}$	92
PE $_{\alpha}$ -based	PE $_{\alpha=-0.2}$ & PE $_{\alpha=0}$ & PE $_{\alpha=0.1}$	58
FDE $_{\alpha}$ -based	FDE $_{\alpha=-0.2}$ & FDE $_{\alpha=-0.1}$ & FDE $_{\alpha=0}$	91.6
Proposed method	FuzzDE $_{\alpha=-0.1}$ & PE $_{\alpha=-0.2}$ & FuzzDE $_{\alpha=0.1}$ (1 of 15)	100

From Table 4, it can be seen that as the number of features increases, the recognition rates of the feature extraction methods based on FuzzDE $_{\alpha}$, DE $_{\alpha}$ and FDE $_{\alpha}$ all improved, but the fault diagnosis performance is still much less than that of the mixed double features in Table 3, which indicates that different fractional order features with the same entropy still have certain limitations. Furthermore, we can also observe from Table 4 that the mixed feature extraction method proposed in this paper achieves a recognition rate of 100% for 15 combinations when triple features are selected, further demonstrating the excellent performance of the mixed feature extraction method for bearing fault diagnosis. To visualize the specific details of these 15 combinations, Table 5 shows the number of occurrences of each feature in the combinations with 100% recognition rate.

Table 5. Number of occurrences of each feature in the combination of the mixed triple features with 100% recognition rate.

Feature	Appear Times
FuzzDE $_{\alpha=-0.1}$	11
FuzzDE $_{\alpha=-0.2}$	4
PE $_{\alpha=-0.2}$	2
PE $_{\alpha=-0.1}$	3
PE $_{\alpha=0}$	3
PE $_{\alpha=0.1}$	4
PE $_{\alpha=0.2}$	3
FDE $_{\alpha=-0.1}$	6
FDE $_{\alpha=0}$	5
FDE $_{\alpha=0.1}$	4

It is clear from Table 5 that FuzzDE $_{\alpha=-0.1}$ has the highest number of occurrences at 11, far more than any other features, which proves the efficiency of FuzzDE $_{\alpha}$ in bearing fault diagnosis. In addition, among the feature combinations with 100% recognition rate, only DE $_{\alpha}$ is absent, which is due to the fact that FuzzDE is an improvement on DE, further validating the conclusion that FuzzDE is more differentiable than DE. We can also find that although the PE $_{\alpha}$ has a low recognition rate on bearing fault diagnosis, it can accurately

classify some samples that cannot be correctly classified by other entropies. Hence, we can also conclude that different entropies can distinguish different signal classes, and following the mixed feature extraction method proposed in this paper, while selecting mixed fractional order entropies simultaneously can effectively improve the performance of bearing fault diagnosis.

Figure 12 depicts the distribution of the triple features at 100% recognition rate with the combination of $\text{FuzzDE}_{\alpha=-0.1}$, $\text{PE}_{\alpha=-0.2}$ and $\text{FDE}_{\alpha=0.1}$. Compared to Figure 11, we can intuitively find that Figure 12 can perfectly distinguish between IR1 as well as IR2, which are two different sizes of the same fault class, and it is obvious that the mixed double features distribution cannot achieve such results.

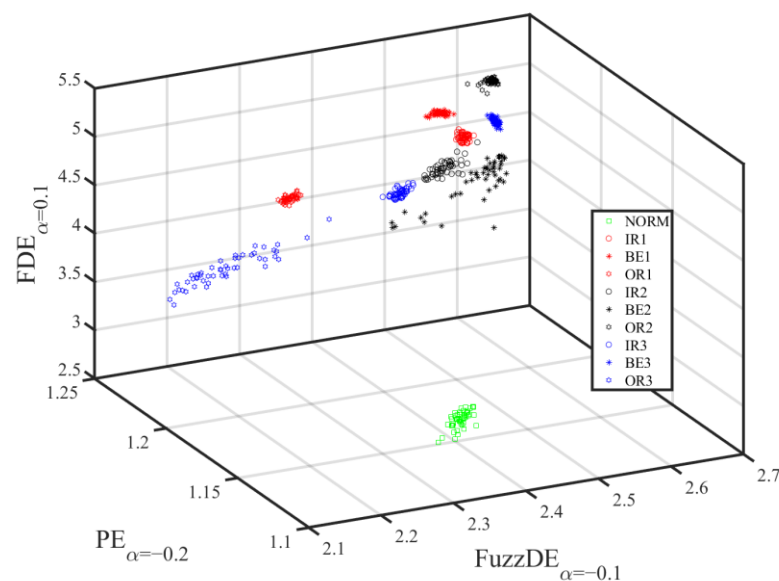


Figure 12. Distribution of the mixed triple features at 100% recognition rate ($\text{FuzzDE}_{\alpha=-0.1}$, $\text{PE}_{\alpha=-0.2}$, $\text{FDE}_{\alpha=0.1}$).

5. Conclusions

In this paper, a new non-linear dynamic parameter is proposed, and a mixed features extraction method is put forward based on this new parameter. The main conclusions are as follows.

1. Fractional order calculation is introduced on the basis of fuzzy dispersion entropy (FuzzDE), and a new entropy called fractional order FDE (FuzzDE_{α}) is proposed. Simulated experiments have shown that compared with FuzzDE, FuzzDE_{α} can provide more features of greater sensitivity to changes in the dynamics of the time series.
2. FuzzDE_{α} is combined with DE_{α} , PE_{α} as well as FDE_{α} to present a mixed features extraction method. For ten classes of bearing signals, the proposed mixed features fault diagnosis method achieves 100% recognition rate at only triple features.
3. Regardless of how many features are selected, the FuzzDE_{α} proposed in this paper is the most effective in fault diagnosis compared to the other three fractional order entropies, where $\text{FuzzDE}_{\alpha=-0.1}$ appears a total of 11 times in the combination of the triple features with the recognition rate of 100%.

Author Contributions: Formal analysis, B.T.; funding acquisition, Y.L.; methodology, B.G.; project administration, B.G.; visualization, S.J.; writing—original draft, B.T.; writing—review and editing, Y.L. All authors have read and agreed to the published version of the manuscript.

Funding: This research was funded by [National Natural Science Foundation of China] grant number [61871318], [Natural Science Foundation of Shaanxi Province] grant number [2022JM-337].

Institutional Review Board Statement: Not applicable.

Informed Consent Statement: Not applicable.

Data Availability Statement: The data used to support the findings of this study are available from the corresponding author upon request.

Conflicts of Interest: The authors declare no conflict of interests.

Nomenclature

FuzzDE	Fuzzy Dispersion Entropy
FuzzDE _α	Fractional order fuzzy dispersion entropy
PE	Permutation entropy
PE _α	Fractional order permutation entropy
DE	Dispersion entropy
DE _α	Fractional order dispersion entropy
FDE	Fluctuation-based dispersion entropy
FDE _α	Fractional order fluctuation-based dispersion entropy
NCDF	Normal cumulative distribution function
SE	Sample entropy
FRDE	Fluctuation-based reverse dispersion entropy
RDE	Reverse dispersion entropy
FuzzEn	Fuzzy entropy
RCMDE	Refined composite multiscale dispersion entropy
GRCMFDE _α	Generalized refined composite multiscale fluctuation-based fractional dispersion entropy
LM	Linear mapping
TANSIG	Tangent sigmoid
LOGSIG	Logarithm sigmoid
SORT	Sorting method

References

- Berger, A.L.; Della Pietra, V.J.; Della Pietra, S.A. A maximum entropy approach to natural language processing. *Comput. Linguist.* **1996**, *22*, 39–71.
- Martyushev, L.M.; Seleznev, V.D. Maximum entropy production principle in physics, chemistry and biology. *Phys. Rep.* **2006**, *426*, 1–45. [[CrossRef](#)]
- Rostaghi, M.; Khatibi, M.M.; Ashory, M.R.; Azami, H. Bearing Fault Diagnosis Using Refined Composite Generalized Multiscale Dispersion Entropy-Based Skewness and Variance and Multiclass FCM-ANFIS. *Entropy* **2021**, *23*, 1510. [[CrossRef](#)] [[PubMed](#)]
- Zhang, X.; Liang, Y.; Zhou, J.; Zang, Y. A novel bearing fault diagnosis model integrated permutation entropy, ensemble empirical mode decomposition and optimized SVM. *Measurement* **2015**, *69*, 164–179. [[CrossRef](#)]
- Yan, R.; Liu, Y.; Gao, R. Permutation entropy: A nonlinear statistical measure for status characterization of rotary machines. *Mech. Syst. Signal Process.* **2012**, *29*, 474–484. [[CrossRef](#)]
- Zhang, X.; Wang, H.; Ren, M.; He, M.; Jin, L. Rolling Bearing Fault Diagnosis Based on Multiscale Permutation Entropy and SOA-SVM. *Machines* **2022**, *10*, 485. [[CrossRef](#)]
- Ying, W.; Tong, J.; Dong, Z.; Pan, H.; Liu, Q.; Zheng, J. Composite Multivariate Multi-Scale Permutation Entropy and Laplacian Score Based Fault Diagnosis of Rolling Bearing. *Entropy* **2022**, *24*, 160. [[CrossRef](#)]
- Rostaghi, M.; Azami, H. Dispersion Entropy: A Measure for Time Series Analysis. *IEEE Signal Process. Lett.* **2016**, *23*, 610–614. [[CrossRef](#)]
- Gu, C.; Qiao, X.; Li, H. Misfire Fault Diagnosis Method for Diesel Engine Based on MEMD and Dispersion Entropy. *Shock Vib.* **2021**, *5*, 1–14. [[CrossRef](#)]
- Azami, H.; Fernandez, A.; Escudero, J. Multivariate Multiscale Dispersion Entropy of Biomedical Times Series. *Entropy* **2017**, *21*, 913. [[CrossRef](#)]
- Azami, H.; Escudero, J. Amplitude- and Fluctuation-Based Dispersion Entropy. *Entropy* **2018**, *20*, 210. [[CrossRef](#)] [[PubMed](#)]
- Li, Y.; Gao, X.; Wang, L. Reverse Dispersion Entropy: A New Complexity Measure for Sensor Signal. *Sensors* **2019**, *19*, 5203. [[CrossRef](#)] [[PubMed](#)]
- Li, Y.; Jiao, S.; Gao, X. A novel signal feature extraction technology based on empirical wavelet transform and reverse dispersion entropy. *Def. Technol.* **2021**, *17*, 1625–1635. [[CrossRef](#)]
- Jiao, S.; Geng, B.; Li, Y. Fluctuation-based reverse dispersion entropy and its applications to signal classification. *Appl. Acoust.* **2021**, *175*, 107857. [[CrossRef](#)]

15. Rostaghi, M.; Khatibi, M.M.; Ashory, M.R.; Azami, H. Fuzzy Dispersion Entropy: A Nonlinear Measure for Signal Analysis. *IEEE Trans. Fuzzy Syst.* **2022**, *30*, 3785–3796. [[CrossRef](#)]
16. Ali, K. Fractional order entropy: New perspectives. *Opt.-Int. J. Light Electron Opt.* **2016**, *127*, 9172–9177.
17. Ingo, C.; Magin, R.L.; Parrish, T.B. New Insights into the Fractional Order Diffusion Equation Using Entropy and Kurtosis. *Entropy* **2014**, *16*, 5838–5852. [[CrossRef](#)] [[PubMed](#)]
18. Zunino, L.; Pérez, D.G.; Martín, M.T. Permutation entropy of fractional Brownian motion and fractional Gaussian noise. *Phys. Lett. A* **2008**, *372*, 4768–4774. [[CrossRef](#)]
19. He, S.; Sun, K. Fractional fuzzy entropy algorithm and the complexity analysis for nonlinear time series. *Eur. Phys. J. Spec. Top.* **2018**, *227*, 943–957. [[CrossRef](#)]
20. Zheng, J.; Pan, H. Use of generalized refined composite multiscale fractional dispersion entropy to diagnose the faults of rolling bearing. *Nonlinear Dyn.* **2021**, *101*, 1417–1440. [[CrossRef](#)]
21. Li, Y.; Mu, L. Particle Swarm Optimization Fractional Slope Entropy: A New Time Series Complexity Indicator for Bearing Fault Diagnosis. *Fractal Fract.* **2022**, *6*, 345. [[CrossRef](#)]
22. Azami, H.; Escudero, J. Improved multiscale permutation entropy for biomedical signal analysis: Interpretation and application to electroencephalogram recordings. *Biomed. Signal Process. Control* **2016**, *23*, 28–41. [[CrossRef](#)]
23. Azami, H.; Fernandez, A.; Escudero, J. Refined Multiscale Fuzzy Entropy based on Standard Deviation for Biomedical Signal Analysis. *Med. Biol. Eng. Comput.* **2017**, *55*, 2037–2052. [[CrossRef](#)] [[PubMed](#)]
24. Wu, G.; Baleanu, D. Chaos synchronization of the discrete fractional logistic map. *Signal Process.* **2014**, *102*, 96–99. [[CrossRef](#)]
25. Li, Y.; Liu, F.; Wang, S. Multi-scale Symbolic Lempel-Ziv: An Effective Feature Extraction Approach for Fault Diagnosis of Railway Vehicle Systems. *IEEE Trans. Ind. Inform.* **2021**, *17*, 199–208. [[CrossRef](#)]
26. Case Western Reserve University. Available online: <http://csegroups.case.edu/bearingdatacenter/pages/download-data-file> (accessed on 1 July 2022).